Electrically injected InGaAs/GaAs photonic crystal membrane light emitting microcavity with spatially localized gain

Yong K. Kim,[1] Victor C. Elarde,[2] Christopher M. Long,[3] James J. Coleman,[3] and Kent D. Choquette[3,a)]

[1]*Intel Corporation, 2200 Mission College Blvd., Santa Clara, California 95054, USA*
[2]*QPC Lasers, Inc., 15632 Roxford Street, Sylmar, California 91342, USA*
[3]*Electrical and Computer Engineering, University of Illinois, 208 N. Wright Street, Urbana, Illinois 61801, USA*

Electrically injected photonic crystal membrane light emitting microcavities with spatially localized optical gain are reported. The localization of the InGaAs quantum well inside the defect cavity of the photonic crystal allows for efficient coupling of the optical mode to the gain medium and reduces nonradiative carrier recombination. The use of a buried oxide layer under the semiconductor membrane enables optical and electrical confinement and a submicron diameter oxide aperture provides a current path. Enhancement of the electroluminescence intensity is observed as a result of the spatial localization of the quantum well, and the spectral characteristics at room temperature indicate the photonic crystal microcavity confinement. © *2008 American Institute of Physics.*
[DOI: 10.1063/1.3040690]

I. INTRODUCTION

Microcavity lasers are of interest in quantum optics and may have application in quantum information, inter- and intrachip communications, and environmental sensing applications. Two-dimensional photonic crystal confinement within a thin semiconductor membrane has been used to confine light within a defect to volumes of a few to less than a cubic wavelength of the photon.[1–14] Electrical injection for photonic crystal membrane lasers is desirable because diode operation is intrinsically more efficient and practical than photopumped devices. An electrically injected nanophotonic emitter must provide low optical and electrical losses and also provide mechanical stability, high thermal conductivity, and a low resistance current path that minimally perturbs the optical modes of the cavity. However, photonic crystal membrane lasers developed to date have been nearly exclusively demonstrated by photoexcitation.[5–14] It is challenging to employ a *p-n* junction in the photonic crystal microcavity without degrading the optical quality factor, although electrical injection has been demonstrated in large area band-edge photonic crystal lasers,[1] edge-emitting quantum dot photonic crystal lasers,[2] and air-suspended photonic crystal defect lasers with a central post.[3,4] The smallest photonic crystal membrane laser diodes to date employ the latter structure where the central post at the center provides a current path.[4] The majority of photonic crystal membrane lasers (either photopumped or electrically injected) are composed of InGaAsP alloys and nominally emit at 1500 nm. This material system provides low nonradiative recombination velocity at the etched hole sidewalls as compared with AlGaAs materials. This is particularly important because of the large surface area exposed inside of the many air holes where nonradiative recombination can occur.

We report on GaAs/InGaAs electrically injected photonic crystal membrane light emitters with spatially localized optical gain at 1020 nm. The microcavity membrane devices are on top of an oxide layer for optical and electrical confinement with a submicron diameter unoxidized aperture to provide a current path. By restricting the quantum well to extend only within the photonic crystal defect, the concomitant nonradiative carrier recombination at the etched holes can be eliminated, producing enhanced optical gain. Nevertheless, the relatively high optical loss significantly reduces the cavity quality factor,[15] although the effects of the photonic crystal cavity can be observed in electroluminescence. We first describe the growth and fabrication of the spatially localized gain photonic crystal membrane devices, and then report the electrical and optical properties measured at room temperature. We conclude with a summary and discussion of requirements for laser operation.

II. DESIGN AND FABRICATION

The electrically injected photonic crystal membrane device structure is sketched in Fig. 1. It consists of a photonic crystal membrane composed of GaAs/InGaAs layers over a buried oxide layer with a central unoxidized aperture to provide a current path through the insulating oxide. This structure can be mechanically stable and provide improved heat sinking,[15] resulting in continuous-wave operation by photopumping at room temperature.[5] A disadvantage of the underlying oxide is the reduced vertical optical confinement from total internal reflection in the membrane at the membrane/oxide interface. In addition, a circularly symmetric cavity is preferable for the selective oxidation process,[16] such as a hexagonal (*H*) defect, although line defect heterostructure cavities have exhibited higher quality factor.[17] By restricting the quantum well active medium to the area inside the photonic crystal defect through selective area epitaxy[18] or quan-
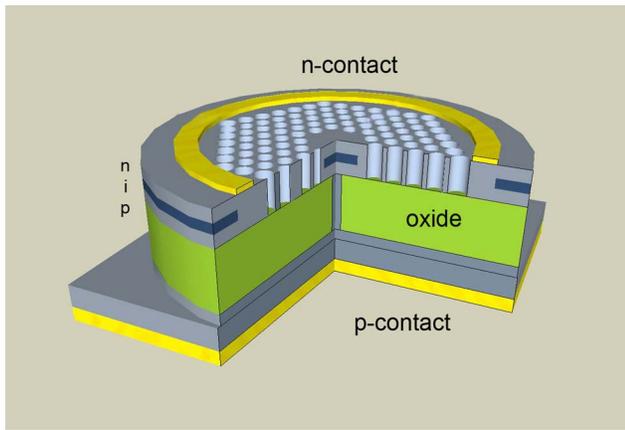

FIG. 1. (Color online) A schematic of the electrically injected photonic crystal light emitter. The patterned quantum well is placed above the oxide aperture within the hexagonal defect of the photonic crystal.

FIG. 2. (Color online) (a) Optical image and (b) scanning electron microscope image of a photonic crystal membrane light emitting diode.

tum well patterning, we can enhance the coupling between the gain and the optical modes and avoid carrier loss associated with nonradiative recombination. Spatially localizing the quantum well gain is material independent and thus enables photonic crystal membrane emitters in the InGaAs/GaAs semiconductor system. Note also that this approach will allow integration of low loss passive waveguides with the microcavity emitters.

The epitaxial structure is grown in a two-step metal organic chemical vapor deposition process. The base layers consist of a 250 nm *p*-type heavily doped AlAs layer, a 101.5 nm undoped GaAs layer, a 7 nm InGaAs quantum well, and a 10 nm thick GaAs cap layer, all grown on a *p*-type (100) GaAs wafer. The quantum well is designed to have an electroluminescence peak near 1020 nm. The sample is removed from the growth reactor and gold alignment marks for subsequent electron beam lithography and optical lithography are defined. Electron beam lithography is next used to pattern an etch mask of polymethylmethacrylate (PMMA). The mask is used for selective removal of the quantum well within the photonic crystal region surrounding the defect cavity by a wet etchant. After removing the PMMA, the sample is returned to the reactor for overgrowth of a 51.5-nm-thick undoped GaAs layer and a 40 nm Si-doped GaAs contact layer.

After the epitaxial growth, a layer of SiO_2 is deposited and the photonic crystal hole patterns surrounded by oxidation trenches are simultaneously defined by a second electron beam lithography step. The photonic crystal defect is aligned to coincide with the previously patterned quantum well. The defined patterns are transferred to the SiO_2 layer and the trenches are first etched by inductively coupled plasma reactive ion etching. The exposed AlAs at the sidewall of the trench is oxidized at 370 °C to form a buried oxide layer under the membrane.[16] The oxide apertures are thus self-aligned to the center of the photonic crystal defect. The photonic crystal patterns are then etched into the GaAs membrane by a second inductively coupled plasma reactive ion etch process. Lastly, the top and backside metal contacts are deposited and annealed. The completed photonic crystal device surrounded by a top metal contact is shown in Fig. 2.
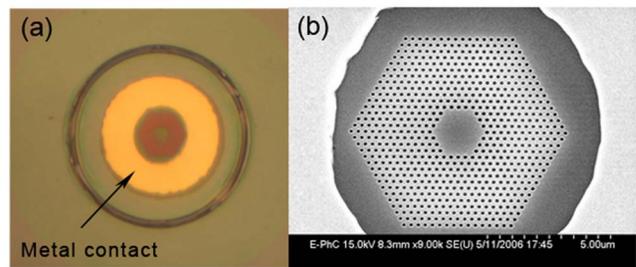
An array of photonic crystal microcavities, comprised of different lattice constants from 250 to 325 nm and different trench diameters differing by an increment of 200 nm, is defined. The hole radius to lattice constant ratio of all photonic crystals is fixed to 0.32. Various sized hexagonal defect cavities are fabricated, and 12 periods of the photonic crystal holes surround each defect. Shown in Fig. 2(b) is a hexagonal defect cavity with four holes missing along each side (*H*4). The photonic crystal pattern is designed to create a photonic band gap around the emission spectrum of the quantum well, where the varying lattice constant will spectrally scan the cavity resonances across the gain bandwidth.

III. DEVICE CHARACTERIZATION

The photonic crystal membrane light emitters are probe tested at room temperature using dc and pulsed current injection. The light emission is captured with an optical fiber suspended over the cavity which is connected into an optical spectrum analyzer. Due to the very low emission output, device spectra are obtained using a relatively wide 5 nm spectrometer resolution bandwidth.

Figure 3 shows a dc current-voltage characteristic for devices with a current aperture diameter of 400 nm. The devices exhibit a differential electrical resistance of approximately 650 kΩ due to the transit of electrons through the photonic crystal pattern and the transport of holes through the narrow current aperture. Figure 4 shows the comparison between the electroluminescence observed from an unetched quantum well sample, a quantum well sample penetrated by an etched photonic crystal, and a spatially localized quantum well surrounded by an etched photonic crystal. The latter two samples have an oxide aperture diameter of 400 ± 200 nm in Fig. 4, which is smaller than the *H*4 microcavity diameter. The diameter uncertainty of these devices arises from the
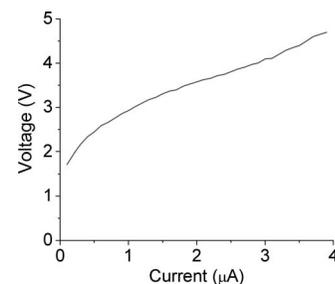

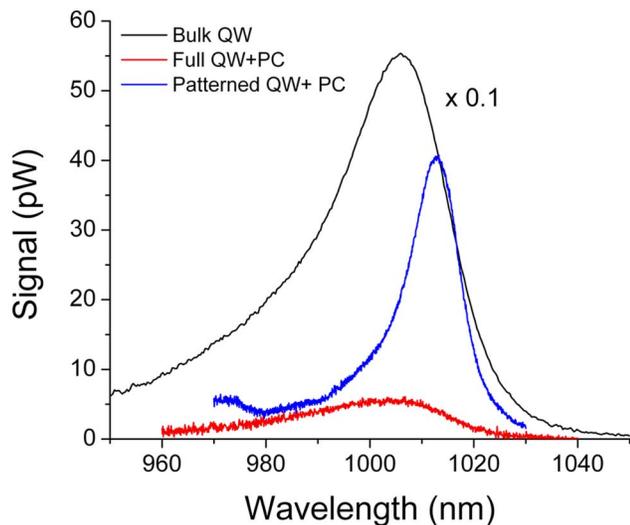FIG. 3. Current vs voltage characteristics of a device with a 400 nm diameter oxide aperture.

FIG. 4. (Color online) Electroluminescence spectra obtained from a bulk quantum well (dashed), photonic crystal with a perforated quantum well (shaded), and photonic crystal with the patterned quantum well in the defect (solid). Both photonic crystal devices are measured at a 7 μA bias current.

200 nm step between trench diameters, as noted above. The electroluminescence from the unpatterned quantum well sample is emitted from a square etched mesa with an oxide aperture side length of 1 ± 0.5 μm, where the uncertainty arises from the 0.5 μm step between square mesas. The electroluminescence spectra from all samples are collected at a 7 μA dc current injection, and both photonic crystal devices have the same lattice constant of 320 nm.

Figure 4 demonstrates that the quantum well electroluminescence is severely diminished when penetrated by the photonic crystal holes. The peak intensity of the patterned quantum well device is approximately eight times greater than that of the perforated quantum well device due to the localization of the quantum well inside of the photonic crystal defect. This shows that the patterned quantum well can reduce nonradiative recombination at the air holes and can also improve the spatial overlap between the optical mode and the optical gain. The maximum electroluminescence from the spatially localized quantum well is reduced by a factor of 0.07 as compared to the unetched quantum well sample in Fig. 4. If nonradiative recombination is absent, the electroluminescence should scale with current density. Note that the cross section active area of the spatially localized quantum well is a factor of 0.125 ± 0.09 less than the unpatterned quantum well. Therefore, although the electroluminescence ratio between the spatially localized quantum well device and the unetched quantum well device falls within the expected scaling range, it is likely that nonradiative recombination is still present for the former.

The dc electroluminescence spectra shown in Fig. 5 demonstrate the effect of the photonic crystal microcavity. Spectra obtained from $H4$ photonic crystal microcavities with an oxide aperture of 400 nm and approximately 15 μm current injection are measured for a photonic crystal lattice constant varying from 290 to 320 nm. There are two cavity modes observed in the electroluminescence spectra in Fig. 5, where spectral tuning of over 30 nm is observed by changing
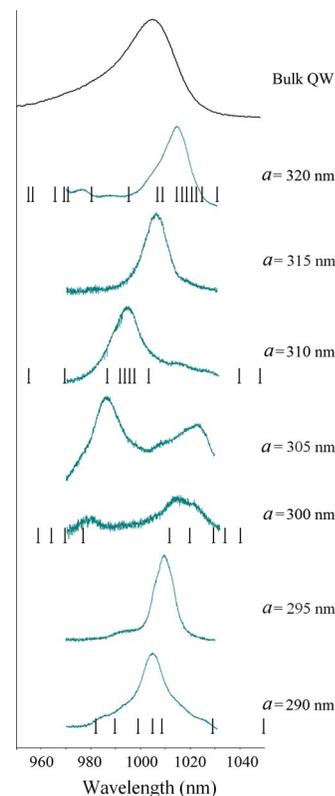

FIG. 5. (Color online) Electroluminescence spectra vs lattice spacing a of the $H4$ photonic crystal defects with fixed hole radius/lattice spacing ratio of 0.32 and 400 nm oxide aperture at 15 μA. Vertical bars indicate the positions of calculated resonant modes for a=290, 300, 310, and 320 nm.

the photonic crystal lattice spacing. Increasing the lattice spacing of the photonic crystal shifts the cavity modes toward longer wavelengths as expected.[12,19] Note that the cavity resonances observed all fall within the spectral bandwidth of the bulk quantum well electroluminescence, which is also shown in Fig. 5. The signal intensity measured from the photonic crystal cavity with a lattice constant of 300 nm is significantly weaker than other spectra because the cavity modes do not align well with the gain spectrum.

A three-dimensional finite-difference time-domain simulation is performed on the $H4$ photonic crystal structure with nine periods of etched holes surrounding the central cavity. The membrane is bounded by air on top and an oxide underneath with a 400 nm diameter current aperture. The simulation domain has 20 grid points per lattice period, and the air hole radii are set at 0.325 times the lattice period. The vertical lines added to the spectra in Fig. 5 indicate the calculated positions of the cavity resonances. Comparison of the simulation resonances and the measured modes shows general agreement and indicates that the measured spectra result from several closely spaced microcavity resonances.

The photonic crystal microcavities are designed to match their photonic band gap to the emission spectrum of the quantum well. The measured cavity modes for two $H4$ defect devices (with differing oxide aperture diameter) and the quantum well gain bandwidth are plotted as a function of the lattice spacing in Fig. 6. The solid lines are the calculated photonic band edges as a function of membrane thickness normalized to the lattice period. As the lattice spacing in-
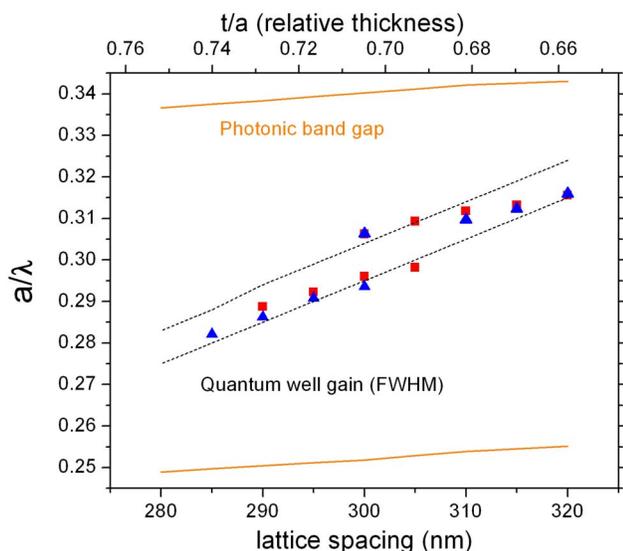
FIG. 6. (Color online) Resonant frequencies of the cavity modes as a function of the lattice spacing (bottom axis) and relative membrane thickness (upper axis). The solid lines represent the calculated edges of the photonic bandgap; the open squares (closed triangles) show the cavity modes of a 400 nm (600 nm) oxide aperture device; the dotted lines correspond to the quantum well gain bandwidth.

creases, the normalized membrane thickness (t/a) decreases, and the boundaries of the photonic band gap increase. The electroluminescence emission from the photonic crystal defect cavities all fall within the photonic band gap and within the quantum well gain bandwidth, as expected.

The cavity modes in the photonic crystals with a 600 nm oxide aperture vary slightly from the cavity modes with a 400 nm oxide aperture in Fig. 6. This difference may be caused by the slightly larger oxide aperture size and the position of the oxide aperture. As the oxide aperture increases, the optical loss of the cavity should increase because the optical mode at the oxide aperture is not as strongly confined in the vertical direction.[3,4] Thus, the normalized frequencies of the 600 nm oxide aperture devices (triangles) are slightly smaller than those of the 400 nm oxide aperture devices (squares) in Fig. 6.

IV. CONCLUSIONS

Photonic crystal membrane light emitting diodes with spatially localized gain have been fabricated and characterized. Employing spatially localized optical gain provides greater flexibility in semiconductor materials, and in this case the InGaAs/GaAs quantum wells emitting nominally at 1020 nm are used. The localization of the quantum well allows for efficient coupling of the cavity mode to the gain medium and reduces nonradiative recombination at the semiconductor/air interfaces within the photonic crystal air holes. This approach will also enable the integration of active devices with gain (such as light emitters and detectors) and with passive elements (such as waveguides or splitters). Ultimately gain patterning could be accomplished on a nanometer scale[18] and thus allows modal engineering by creating gain precisely at an antinode of the desired optical mode. Significant enhancement of the electroluminescence intensity

is observed as a result of the spatial localization of the quantum well. The use of a submicron diameter oxide aperture enables electrical current injection into the cavity, and the buried oxide layer provides heat sinking and mechanical stability.

In spite of the improved electroluminescence, no stimulated emission is observed under pulsed or dc current injection. In order to achieve electrically injected photonic crystal defect laser diodes, the material gain must be increased and the optical loss must be decreased. Obviously multiple quantum wells can be used, although a thicker etch thickness will reduce the pattern fidelity with the present approach for defining the localized gain. The cavity quality factors extracted from the emission half-widths in Fig. 5 are low, varying from 60 to 100, significantly less than those observed from air-suspended photonic crystal membrane lasers. The broad line shapes in Fig. 5 are partially due to the wide spectrometer resolution bandwidth needed to detect the low intensity emission. However, a relatively low cavity quality factor is expected in our present devices. The reduced vertical confinement due to the underlying oxide layer and the unoxidized central aperture will lead to greater radiation loss. This loss could be improved by using a thicker oxide to discourage modes from coupling into the underlying substrate.[15] Other cavities, such as heterostructures[14] or line defects,[17] may provide enhanced cavity quality factor. Finally, free carrier absorption from the doped regions of the membrane will also adversely affect the quality factor, although clearly a trade-off exists between carrier transport (resistance) and optical loss. An increase in the cavity quality factor with refined microcavity design as well as an increase in the localized gain should lead to robust photonic crystal membrane laser diodes.

[1]M. Imada, S. Noda, A. Chutinan, T. Tokuda, M. Murata, and G. Sasaki, Appl. Phys. Lett. **75**, 316 (1999).
[2]J. Topoll'ancik, S. Pradhan, P.-C. Yu, S. Ghosh, and P. Bhattacharya, IEEE Photonics Technol. Lett. **16**, 960 (2004).
[3]H. G. Park, S. H. Kim, S. H. Kwon, Y. G. Ju, J. K. Yang, J. H. Baek, S. B. Kim, and Y. H. Lee, Science **305**, 1444 (2004).
[4]H. G. Park, S. H. Kim, M. K. Seo, Y. G. Ju, S. B. Kim, and Y. H. Lee, IEEE J. Quantum Electron. **41**, 1131 (2005).
[5]O. Painter, R. K. Lee, A. Scherer, A. Yariv, J. D. O'Brien, P. D. Dapkus, and I. Kim, Science **284**, 1819 (1999).
[6]J. K. Hwang, H. Y. Ryu, D. S. Song, I. Y. Han, H. W. Song, J. K. Park, and Y. H. Lee, Appl. Phys. Lett. **76**, 2982 (2000).
[7]C. Monat, C. Sessal, X. Letartre, P. Viktorovitch, P. Regreny, and P. Gendry, Electron. Lett. **37**, 764 (2001).
[8]P. T. Lee, J. R. Cao, S. J. Choi, Z. H. Wei, J. D. O'Brien, and P. D. Dapkus, Appl. Phys. Lett. **81**, 3311 (2002).
[9]H. G. Park, J. K. Hwang, J. Huh, H. Y. Ryu, S. H. Kim, J. S. Kim, and Y. H. Lee, IEEE J. Quantum Electron. **38**, 1353 (2002).
[10]H. G. Park, S. K. Kim, S. H. Kwon, G. H. Kim, S. H. Kim, H. Y. Ryu, S. B. Kim, and Y. H. Lee, IEEE Photonics Technol. Lett. **15**, 1327 (2003).
[11]K. Inoshita and T. Baba, IEEE J. Sel. Top. Quantum Electron. **9**, 1347 (2003).
[12]Y. S. Choi, S. K. Kim, S. H. Kim, H. G. Park, Y. H. Lee, I. N. Kaiander,

F. Hopfer, R. L. Sellin, and D. Bimberg, J. Vac. Sci. Technol. B **23**, 252 (2005).

[13]M. H. Shih, W. Kuang, T. Yang, M. Bagheri, Z. J. Wei, S. J. Choi, L. Lu, J. D. O'Brien, and P. D. Dapkus, IEEE Photonics Technol. Lett. **18**, 535 (2006).

[14]A. V. Giannopoulos, C. Long, and K. D. Choquette, Electron. Lett. **44**, 803 (2008).

[15]L. Chen and E. Towe, IEEE J. Sel. Top. Quantum Electron. **12**, 117 (2006).

[16]K. D. Choquette, K. M. Geib, C. I. H. Ashby, R. Tweston, O. Blum, H. Q. Hou, B. E. Hammons, D. Mathes, and R. Hull, IEEE J. Sel. Top. Quantum Electron. **3**, 916 (1997).

[17]Y. Tanaka, T. Asano, and S. Noda, J. Lightwave Technol. **26**, 1532 (2008).

[18]V. C. Elarde, R. Rangarajan, J. J. Borchardt, and J. J. Coleman, IEEE Photonics Technol. Lett. **17**, 935 (2005).

[19]C. Reese, B. Gayral, B. D. Gerardot, A. Imamoglu, P. M. Petroff, and E. Hu, J. Vac. Sci. Technol. B **19**, 2749 (2001).